# Numerical assessment of thermal behaviour of a superconducting bus-bar with a Nuclotron-type cable

ŁUKASZ TOMKÓW [1,2], MACIEJ CHOLEWIŃSKI [2], MARIAN CISZEK [2,3], MACIEJ CHOROWSKI [2]

[1] *Department of Materials Science and Metallurgy*
*University of Cambridge*
*27 Charles Babbage Road, Cambridge, CB3 0FS, United Kingdom*

[2] *Department of Cryogenics and Aerospace Engineering*
*Wrocław University of Science and Technology*
*Wybrzeże Wyspiańskiego 27, 50-370 Wrocław, Poland*

[3] *Institute of Low Temperature and Structure Research*
*Polish Academy of Sciences*
*Okólna 2 str., 50-422 Wrocław, Poland*

*e-mail: lukasz.tomkow@pwr.edu.pl*

**Abstract:** Sections of the superconducting magnets of the SIS100 particle accelerator, under construction at the Facility for Antiproton and Ion Research (FAIR), the Society for Heavy Ion Research (GSI), Darmstadt, are going to be connected with the by-pass lines. Each line will be used to transfer a two-phase helium flow and an electric current. The electric current will be carried by four pairs of superconducting Nuclotron-type cables. Fast-ramping currents are expected to cause the generation of heat within the cables. In this work the results of a numerical thermal analysis of a bus-bar are presented. The amount of heat transferred from the environment was found based on geometric dimensions of the line and applied insulation. The amount of hysteresis loss, generated in the cable during the operation under most demanding regime of the operation of the accelerator, was calculated. According to the amount of the generated heat, the amount of the hysteresis loss is low in relation to the heat generated in the superconducting magnets. Also it was found that the cable used in the line still retains a large margin of current-carrying capacity.

**Key words:** electro-thermal analysis, heat transfer, particle accelerators, superconducting bus-bars, superconductivity

## 1. Introduction

The particle accelerator, SIS100, is currently constructed as the major part of the FAIR facility in Darmstadt, Germany. It will consist of six sectors with the dipole magnets (sextants), connected with the by-pass lines [1]. The by-pass lines will carry a two-phase helium flow and electric current between the sextants and will supply the quadrupole magnets. Each line will contain four superconducting bus-bars – the pairs of Nuclotron-type cables with NbTi serving as the superconducting material [2, 3].

The heat budget of the accelerator is very low, therefore any heat generation has to be assessed and, if possible, reduced. The cooling power of the cryogenic system of SIS100 will be approximately 34.9 kW at 4 K [4]. It is expected that the major internal source of heat in the accelerator will be AC losses in the superconducting magnets [5]. The losses in the superconducting magnets were calculated numerically [6] and measured experimentally [7]. In this work a numerical approach is employed to predict the heat generation in bus-bars of a by-pass line for SIS100.

## 2. Methods

The superconducting bus-bar in the analyzed by-pass line consists of two Nuclotron-type cables enclosed in a single steel shell. It serves as a thermal shield and mechanical support. The distance between the axes of the cables is 9.5 mm and it is maintained by the spacers made of G10. The external diameter of each cable is 8.28 mm. The geometry of the bus-bar is shown in Fig. 1.
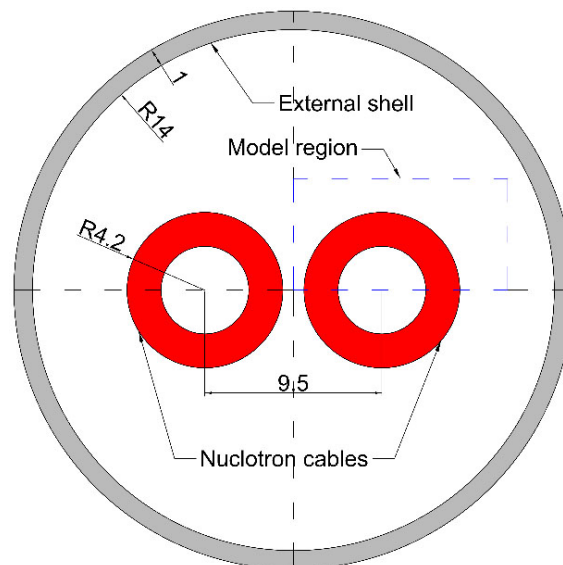


Fig. 1. Geometry of the bus-bar: cross-section of the bus-bar,
modelled region is marked with a blue dashed line

The internal structure of the cable is presented in Fig. 2. The central part of the cable is a cooling tube made of CuNi [8]. The coolant is a two-phase helium flow with a temperature of approximately 4.5 K. The internal diameter of the tube is 4.7 mm, its thickness is 0.5 mm. 23 superconducting strands with NbTi are wound on the tube with a lay pitch of approximately 50 mm [9]. Each strand (diameter of 0.8 mm) contains 32821 superconducting NbTi fine filaments with a diameter of 4 μm, twisted with a twist pitch of 6 mm. The matrix of the composite is copper and the Cu/NbTi ratio is 1.26. The circular layer created by the superconducting strands is fixed with the help of a NiCr fine wire wound with a pitch of 0.6 mm.
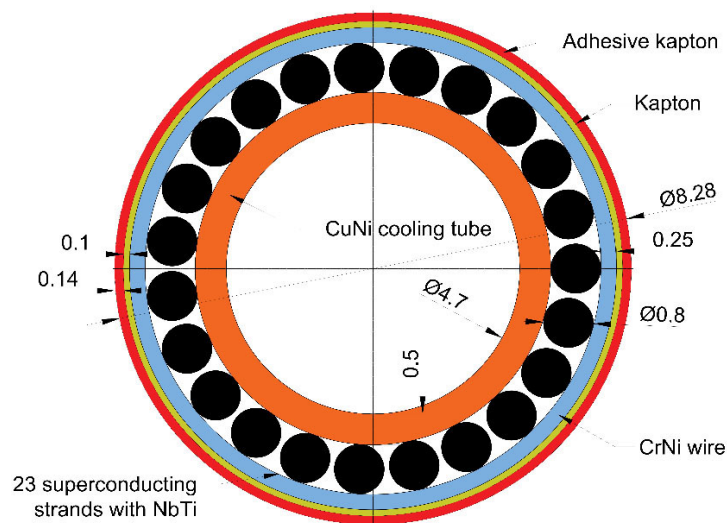


Fig. 2. Geometry of the bus-bar: cross-section of a Nuclotron cable used in SIS100

The array of the superconducting strands is surrounded by the matrix made of a CrNi wire and two layers of Kapton to provide mechanical support and electrical insulation. The strands have a circular cross-section. The design using strands with a trapezoidal cross-section was also considered during the initial phase of the project [10]. The goal of the model is to calculate the heat generation in the superconducting cables of the bus-bar. Since it is expected to be different in each strand, rotational symmetry of a single cable cannot be used to simplify the model. However, the symmetry of the bus-bar allows one to model only a quarter of it, marked with a blue dashed line in Fig. 1. A single cross-section of the bus-bar is modelled in 2D, with currents flowing in the $z$ direction and two components of a magnetic field, $x$ and $y$. Boundary conditions applied in the model are shown in Fig. 3 and described further.

The model is developed in Comsol Multiphysics. The Magnetic Field Formulation module is used to find distribution of the magnetic field, electric current density and heat generation. Heat transfer in the solid module is applied to calculate the temperature and heat transfer in the modelled region. The system is modelled using time-dependent study. The general flowchart of the operation of the model is shown in Fig. 4. The thermal and electromagnetic calculations are coupled twofold. The electromagnetic heat generation found with the electromagnetic model is
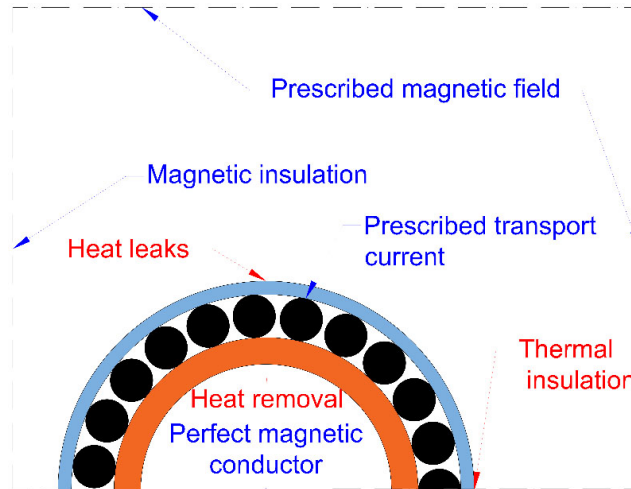
Fig. 3. Boundary conditions used in the model: text in red refers to thermal
boundary conditions, blue – electromagnetic

fed to the thermal model as a heat source. The temperature calculated with the thermal model affects critical current density applied in the electromagnetic model.
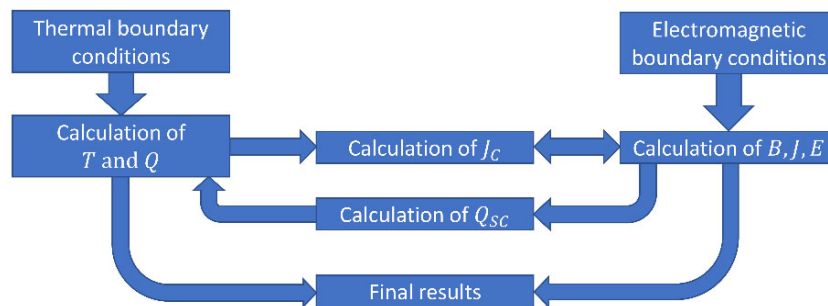


Fig. 4. Flowchart of the numerical model

To model the electromagnetic interactions between the cables in the bus-bar, the electromagnetic boundary conditions are found as the value of the magnetic field generated by the two point currents of 1 A with a reverse directions, located in the axes of the cables. The strength of the magnetic field in the locations corresponding to the boundaries of the model region was read and fitted to generate the shape function $\Gamma(x, y)$.

The accelerator is going to operate under several regimes, with the most demanding one being the training regime [7]. In this case the triangular current $I_{ap}(t)$ is applied, the same as analyzed in the context of SIS100 main magnets [11] and the shells of the bus-bars at the transfer lines [12]. Its frequency is 1 Hz and it oscillates between 0 and 13 kA, giving a very high current change rate of 26 kA/s. Therefore, the significant AC heat generation can be expected in the superconductor.

To find a magnetic field on the boundary of the modelled region $H_b(t, x, y)$ Formula (1) is used.

$$H_b(t, x, y) = \Gamma(x, y) \cdot I_{ap}(t). \tag{1}$$

To calculate the magnetic field the slightly modified H-formulation was used, previously described by Pecher *et al*. [13] and Brambilla *et al*. [14]. The base formula of the model is Faraday's law in the form of Equation (2).

$$\mu_o \left( \frac{\partial H}{\partial t} \right) + \nabla \times E = 0, \tag{2}$$

where: $\mu_o$ is the magnetic constant, $H$ is the magnetic field, $E$ denotes the electric field, which in the case of the considered geometry has a single component $z$. Distribution of the electric currents $J$ is found with Formula (3), yielding a single component of the electric current density $J_z$.

$$J = \nabla \times H. \tag{3}$$

Non-linear behaviour of the electric field in the superconducting material is reflected with Formula (4), applied on the superconducting region as a material parameter.

$$E_z = E_0 \left[ \frac{J_z - J_c}{J_c} \cdot \theta \left( J_z - J_c \right) \right]^n, \tag{4}$$

where: $E_0$ is a certain threshold electric field, $J_c$ is the critical current density, $\theta$ is the Heaviside step function and $n$ is the exponent for power law. The electric field in the remaining part of the region is described with Formula (5). $\rho$ in this formula is the electric resistivity of a material.

$$E_z = \rho \cdot J_z. \tag{5}$$

Twofold connection exists between the electromagnetic and thermal models. The first is the dependence of $J_c$ on both the magnetic induction $B$ and temperature $T$. The behaviour of NbTi in the wires is well described and the Bottura fit was used to calculate $J_c$ [15]. It is described with Formula (6).

$$J_c = \lambda \cdot \frac{C_0}{B} b^\alpha (1 - b)^\beta \left( 1 - t_r^\xi \right)^\gamma. \tag{6}$$

In this formula $C_0, \alpha, \beta, \xi$ and $\gamma$ are the constants assumed as $25 \cdot 10^{10}$ A·T·m$^{-2}$, 0.8, 0.89, 1.7 and 1.87, respectively, based on [16] and fitting to experimental results. $b$ is the reduced magnetic induction found with Formula (7).

$$b = \frac{B}{B_{c2}(T)}. \tag{7}$$

$B_{c2}$ is the critical magnetic induction calculated with Equation (8).

$$B_{c2}(T) = B_0 \left( 1 - t_r^\xi \right). \tag{8}$$

$B_0$ is the critical magnetic induction when the temperature is 0 K, assumed as 14.25 T and $t_r$ in both Formulas, (8) and (6), is the reduced temperature calculated with Equation (9).

$$t_r = \frac{T}{T_0}, \tag{9}$$

where: $T_0$ is the critical temperature when the magnetic induction is 0 T, assumed as 9.35 K. $\lambda$ is the filling parameter calculated with Formula (10).

$$\lambda = N \cdot \frac{a^2}{w^2}. \tag{10}$$

In the above formula $N$ is the number of filaments in the strand, $a$ is the radius of a single filament and $w$ is the radius of the strand.

The general formula for the heat behaviour of the modelled system takes the form of Equation (11). The equation also shows how the change of temperature of an element is calculated.

$$q_g = \rho_v c_p \frac{\partial T}{\partial t} + \nabla q_s, \tag{11}$$

where: $q_g$ is the heat generation per unit volume, $\rho_v$ is the volumetric density of a material and $c_p$ is its heat capacity. It is assumed that the dominant mechanism of the heat transfer inside the cable is heat conduction through solids $q_s$. It is described with Formula (12).

$$q_s = -k_c \nabla T, \tag{12}$$

where $k_c$ is the thermal conductivity of a material.

It is assumed that the initial temperature everywhere in the model is 4.5 K. The boundaries of the thermal model are the external surface of the cable, the interior surface of the cooling pipe and the horizontal cross-section of the cable. To maintain the symmetry of the model, the condition of the thermal insulation is placed on the cross-section line. The heat leaks per unit length to the external surface of the cable are calculated using a radiation model of the entire cryogenic line and are found to be 0.0125 W·m$^{-1}$. The value used is the average radiation heat transfer to the cable. The heat removed by helium in the cooling pipe per unit length $q_{\text{He}}$ is calculated with Formula (13).

$$q_{\text{He}} = h_{\text{He}} \left( T_p - T_{\text{He}} \right), \tag{13}$$

where $T_p$ is the temperature of the surface of the cooling pipe and $T_{\text{He}}$ is the temperature of the coolant in the pipe assumed as 4.5 K. $h_{\text{He}}$ is the convection coefficient calculated with Formula (14), based on [17].

$$h_{\text{He}} = 5.8 \cdot 10^4 \left( T_p - T_{\text{He}} \right)^{1.5}. \tag{14}$$

Two sources of losses in the superconducting strand are considered in the model, the hysteresis losses $q_h$ and coupling losses $q_e$. The local hysteresis losses are found with Formula (15).

$$q_h = E_z \cdot J_z. \tag{15}$$

The calculations of the coupling losses are based on [18]. The size of the coupling losses per unit volume $q_e$ is found with Formula (16).

$$q_e = \frac{B_m^2}{2\mu_0} \cdot \frac{8\tau}{T_m}. \tag{16}$$

In this formula $B_m$ is the local magnitude of the magnetic induction found as the root mean square of the magnetic induction in the entire cross-section of the superconductor, $T_m$ is the half of the cycle period and $\tau$ is the characteristic time found with Formula (17).

$$\tau = \frac{\mu_0}{2\rho_{et}} \cdot \frac{L}{2\pi} \, . \tag{17}$$

In this formula, $L$ is the twist pitch of the strand and $\rho_{et}$ is the effective transverse resistivity of the strand found with Formula (18).

$$\frac{1}{\rho_{et}} = \frac{1}{\rho_t} + \frac{w}{a \cdot \rho_m} + \frac{a \cdot w}{\rho_m} \cdot \left(\frac{2\pi}{L}\right)^2 . \tag{18}$$

$\rho_m$ is the resistivity of matrix. In the considered range of temperatures it is close to constant and independent of temperature. A value of $0.75 \cdot 10^{-9}$ $\Omega$·m was assumed, roughly corresponding with the value for copper with an RRR of 20. $\rho_t$ denotes the effective resistivity of the matrix which, assuming the presence of contact resistance between superconducting filaments and the matrix, is calculated with Formula (19).

$$\rho_t = \rho_m \frac{1 + \lambda}{1 - \lambda} . \tag{19}$$

To find the total losses per meter length, Formula (20) is applied. $\Omega$ represents here the cross-sectional area of the strand.

$$Q_g = \int_\Omega (q_h + q_e) . \tag{20}$$

## 3. Results and discussion

The distribution of magnetic induction in the moment when the current passed through the by-pass line is the highest ($t = 1.5$ s) is shown in Fig. 5. As expected, it is the highest between the cables. It decreases down to zero closer to the axes of the cables. Between the cables the field propagates further into the cable. The critical current density in the superconductor decreases and the shielding current is weaker. It strongly affects the current distribution and heat generation in the cables.

The heat generation per unit volume resulting from the current at $t = 1.5$ s is presented in Fig. 6. The largest heat generation can be observed in the strands closer to the centre of the bus-bar, corresponding with the strength of the magnetic induction affecting the cable. Some artefacts are visible in the figure. However, after integrating the heat generation over the cross-section area of the superconducting strand, they only mildly affect the total heat generation. The total heat generation in the superconducting bus-bar is presented in Fig. 7. It reaches its maximum every half second – either when the current is 13 kA or zero. When the direction of the electric current changes, the heat generation abruptly drops to zero and starts to increase again. As expected, the amount of the dissipated heat depends on the history of the cable, rather than the actual value of the transferred current.
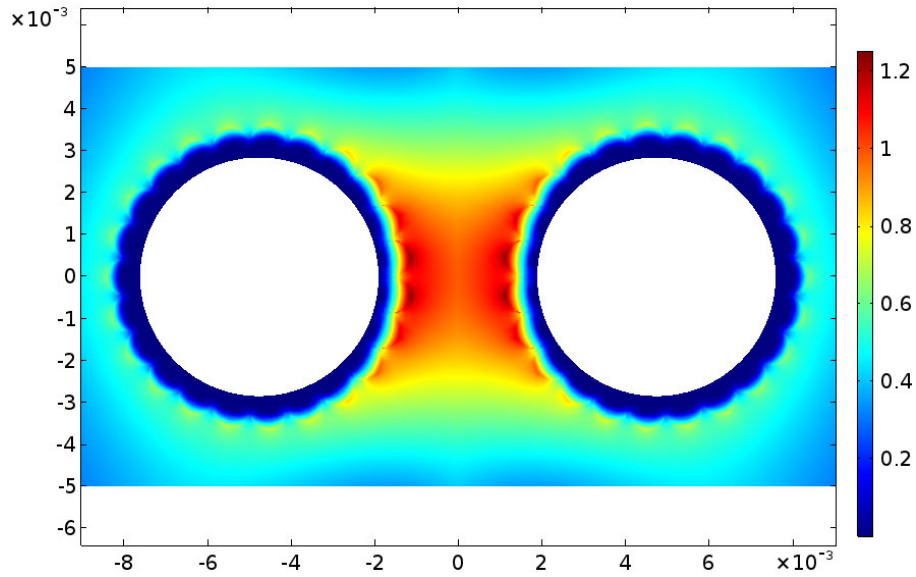
Fig. 5. Results at $t$ = 1.5 s (a single cross-section of a bus-bar is shown):
distribution of the magnetic induction $T$
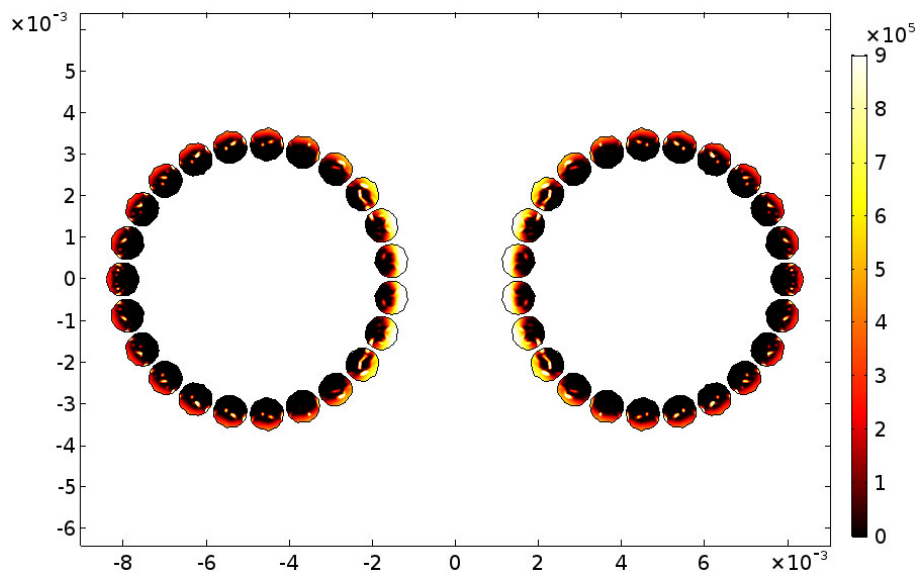


Fig. 6. Results at $t$ = 1.5 s (a single cross-section of a bus-bar is shown):
distribution of the heat generation in the superconducting strands (W·m$^{-3}$)

The initial peak of the heat generation visible in Fig. 7 is very high compared to remaining peaks, as expected with hysteresis losses When the applied electric current is varied the magnetic
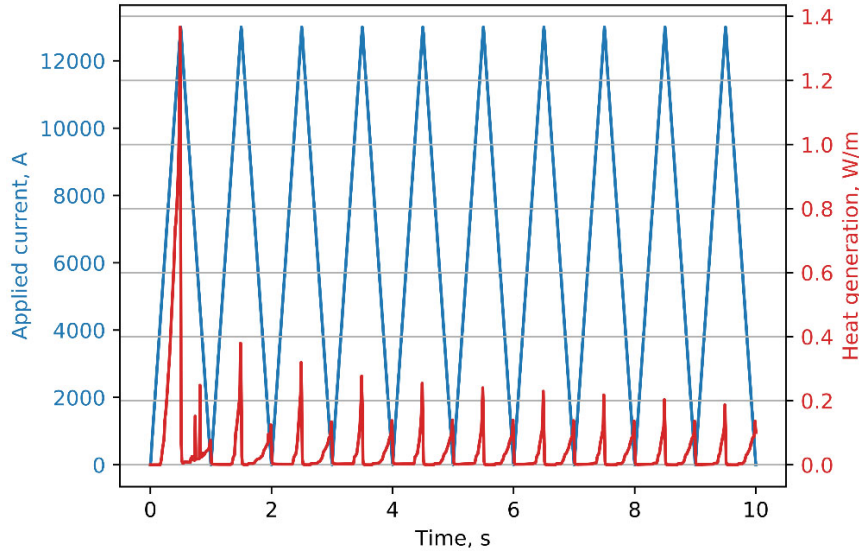
Fig. 7. Applied current and heat generation in the bus-bar as the function of time

field inside the strand also changes causing the appearance of an electric field. In the superconductor the magnetic field changes only where the current is changing. The rest of the volume is shielded.

During the initial cycle a strand is filled with the electric current until the desired value is reached. The current density is equal to the critical current density and a certain fraction of the surface of the strand carries it. Losses appear all over the current-carrying surface, hence the high peak at the beginning of the operation. In each consecutive cycle the losses are lower. In Fig. 7 the peaks occurring during the decrease of the applied current appear to be smaller than during the increase. It is thought to be the effect of the low temporal and mesh resolution of the numerical model. This affects the presence of some artifacts – small regions with a high magnetic field and heat generation. They are especially significant in initially calculated cycles. The difference is reduced with each next cycle. Another explanation is that with the increase of temperature the critical current density of the cable slightly decreases. During the increase of transport current additional regions of the strands start to carry current and an electric field is generated there. Later the distribution of the electric current in the cross-section of the cable stabilizes and the losses in each direction equalize.

The maximum generation of heat during the normal operation of the bus-bar is approximately 2.75 W·m$^{-1}$, the average is 0.79 W/m. This value translates to approximately 68 mJ/cm$^3$ per cycle, the value similar to the ones based on experimental results reported at [19]. The total average hysteresis heat generation in 6 by-pass lines with a length of approximately 45 m each is 213 W. This value is small relative to heat budget of the accelerator, approximately 5% of the total expected heat generation.

The development of temperature for the first 10 s of the operation is presented in Fig. 8. After that thermal behaviour was calculated using the average value of heat generation as an input to the

thermal only model. Thanks to that the computation time was greatly decreased. The calculated increase of the temperature is very small, less than 0.1 K.
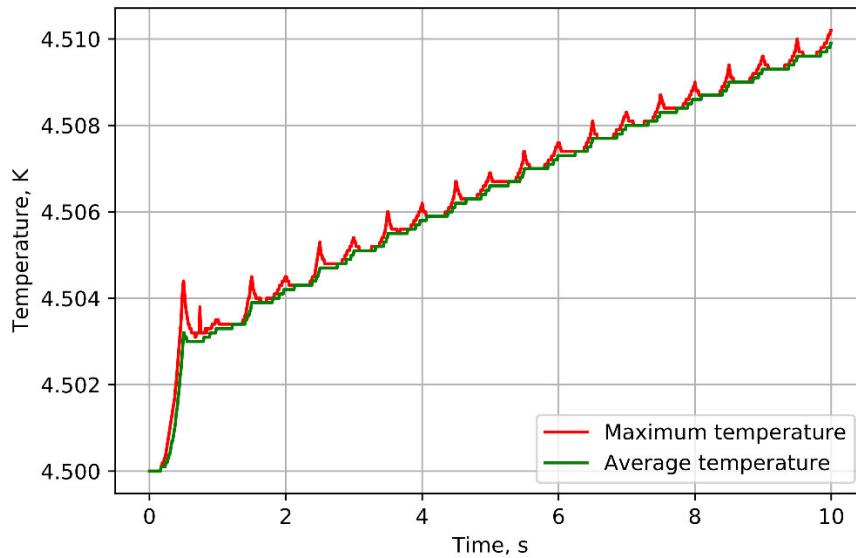


Fig. 8. Maximum and average temperature of the cable versus time

An initial peak in the heat generation affects high increase of temperature during the first 0.5 s of the operation. Later the temperature increases and stabilizes at a low level of approximately 4.56 K.

Fig. 9 shows the distribution of the temperature and heat transfer streamlines after 10 s. The temperature is very homogeneous thanks to a small geometrical size of the cable and relatively
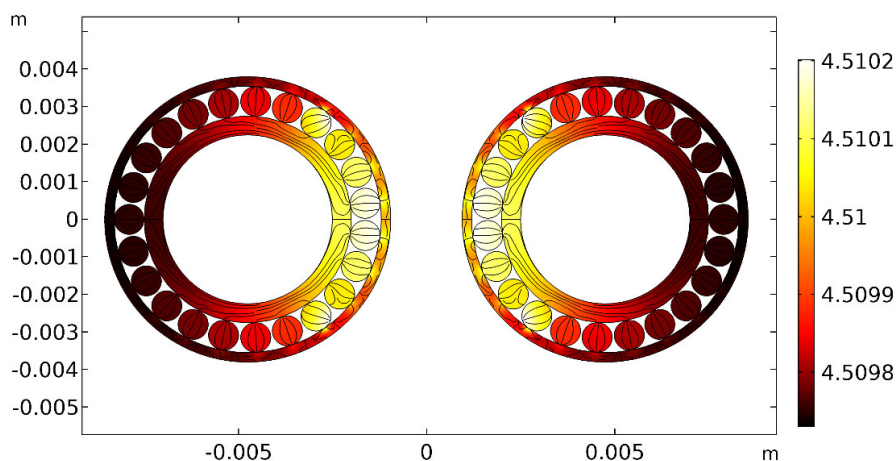


Fig. 9. Temperature distribution after 10 s with heat transfer streamlines marked

large thermal conductivities of materials involved. The warmest parts are the strands closest to the centre of the assembly, since they experience the highest magnetic fields and thus the largest heat generation occurs there.

Cooling with a two-phase helium flow is extremely efficient and is well enough to counter the heat generation. The risk of a quench occurrence is very small compared to the magnets of the accelerator, since the critical current density is high and is only weakly affected by the magnetic field. The parameter of filling of the total critical current is approximately 40%. Additional heat generation will appear from AC losses. Both types of losses were measured experimentally [19]. In the light of the experimental results and numerical ones presented in this paper, the presence of additional losses will not lead to the significant increase of temperature. The calculated value of losses complies with the one obtained experimentally.

# 4. Conclusions

The thermal analysis of a superconducting bus-bar for a by-pass line of the SIS100 accelerator shows that the amount of heat generated in the conditions of a fast-ramped cyclic current does not depend directly on the applied current. Peaks of the heat generation appear in both minima and maxima of the applied current. The heat generation increases when the variations of the applied current cause changes of a magnetic field and thus generate an electric field. The largest heat generation occurs during the initial application of the electric current. Such behaviour agrees with analytical predictions [18].

Based on the obtained results the operation of the superconducting bus-bar is expected to be safe. The risk of quench is very low and the increase of temperature due to the losses in the superconductor is insignificant. The current density margin of the superconducting cable is sufficient. The magnetic field experienced by the cables is low and the resulting critical current densities are high. The applied transport current is less than a half of the capacity of the transfer line. The heat generation is small and agrees with previously reported experimental measurements [19]. The applied cooling method is very efficient and removes any generated heat with minimal increase in temperature.

**References**

[1] Eisel T., Chorowski M., Iluk A., Kauschke M., Kollmus H., Malcher K., Polinski J., Streicher B., *Local Cryogenics for the SIS100 at FAIR*, IOP Conference Series: Materials Science and Engineering, Tucson, AZ, USA, vol. 101, no. 1 (2015), DOI: 10.1088/1757-899X/101/1/012075.

[2] Khodzhibagiyan H.G., Drobin V.M., Fischer E., Kovalenko A.D., Pantsyrny V.I., Potanina L.V., Shikov A.K., Vladimirova N.M., *Design and study of new cables for superconducting accelerator magnets: Synchrotron SIS 100 at GSI and NICA collider at JINR*, Journal of Physics: Conference Series, vol. 234, no. 2 (2010), DOI: 10.1088/1742-6596/234/2/022017.

[3] Acker D., Bleile A., Fischer E., Floch E., Gumenyuk O., Hess G., Kauschke M., Klos F., Knapp T., Leibrock H., Macavei J., Marzouki F., Mierau A., Meier J.P., Moritz G., Muehle C., Mueller H., Pschorn I., Schnizer P., Schroeder C., Shim S.Y., Stafiniak A., Sugita K., Walter F., Weckenmann B., Weipert M., Xiang Y., *Development of FAIR superconducting magnets and cryogenic system*, GSI Scientific Report, no. 506065, pp. 118–119 (2010).

[4] Kauschke M., Xiang Y., Schroeder C.H., Streicher B., Kollmus H., *Cryogenic Supply for Accelerators and Experiments at FAIR*, AIP Conference Proceedings, vol. 1200, no. 2014 (2014).

[5] Fischer E., Schnizer P., Mierau A., Sugita K., Meier J.P., Bleile A., Müller H., Leibrock H., Macavei J., *Status of the Superconducting Magnets for FAIR*, GSI Scientific Report, vol. 24, no. 3, pp. 474–475 (2014).

[6] Fischer E., Kurnyshov R., Shcherbakov P., *Analysis of coupled electromagnetic-thermal effects in superconducting accelerator magnets*, Journal of Physics: Conference Series, vol. 97, pp. 012261, (2008).

[7] Bleile A., Fischer E., Freisleben W., Mierau A., Schnizer P., Szwangruber P., *Thermodynamic properties of the superconducting dipole magnet of the SIS100 synchrotron*, Physics Procedia, vol. 67, pp. 781–78 (2015).

[8] Fischer E., Sugita K., Schnizer P., Khodzhibagiyan H., *Nuclotron-type cables: From fast ramped sc. magnets to multipurpose application*, IEEE Transactions on Applied Superconductivity, vol. 27, no. 4, pp. 1–5 (2017).

[9] Fischer E., *SIS100 Superconducting Magnets Specification Status & Procurement*, MAC-06 (2011).

[10] Khodzhibagiyan H., Alexeev V., Averichev S., Drobin V., Kovalenko A., Smirnov A., Starikov A., Vladimirova N., Moritz G., Fischer E., Potanina L., Shikov A., Vedernikov G., *Design of new hollow superconducting NbTi cables for fast cycling synchrotron magnets*, IEEE Transactions on Applied Superconductivity, vol. 13, no. 2, pp. 3370–3373 (2003).

[11] Fischer E., Kurnyshov R., Shcherbakov P., *Analysis of the eddy current relaxation time effects in the fair sis 100 main magnets*, IEEE Transactions on Applied Superconductivity, vol. 17, no. 2, pp. 1173–1176 (2007).

[12] Tomków Ł., Trojanowski S., Ciszek M., Chorowski M., *Heat generation by eddy currents in a shell of superconducting bus-bars for SIS100 particle accelerator at FAIR*, Archives of Electrical Engineering, vol. 66, no. 4, pp. 705–715 (2017).

[13] Pecher R., McCulloch M., Chapman S., Prigozhin L., *3D-modelling of bulk type-ii superconductors using unconstrained h-formulation*, Proc. EUCAS 2003 (2003).

[14] Brambilla R., Grilli F., Martini L., *Development of an edge-element model for ac loss computation of high-temperature superconductors*, Superconductor Science and Technology, vol. 20, no. 1, pp. 16–24 (2007).

[15] Bottura L., *A practical fit for the critical surface of NbTi*, IEEE Transactions on Applied Superconductivity, vol. 10, no. 1, pp. 1054–1057 (2000).

[16] Hudson P., Yin F., Jones H., *Evaluation of the temperature and magnetic field dependence of critical current densities of multifilamentary superconducting composites*, IEEE Transactions on Magnetics, vol. 17, no. 5, pp. 1649–1652 (1981).

[17] Deev V., Keilin V., Kovalev I., Kondratenko A., Petrovichev V., *Nucleate and film pool boiling heat transfer to saturated liquid helium*, Cryogenics, vol. 17, no. 10, pp. 557–562 (1977).

[18] Wilson M., *Superconducting magnets*, Clarendon Press Oxford (1983).

[19] Potanina L., Pantsyrny V., Shikov A., Salunin N., Gubkin I., Korpusov V., Khodzhibagiyan H., Kovalenko A., Fischer E., Mueller H., Moritz G., *Experimental results on the development of superconducting NbTi/Cu-Mn/Cu wires for magnet systems of SIS100 and SIS300 synchrotrons of FAIR*, IEEE Transactions on Applied Superconductivity, vol. 20, no. 3, pp. 1395–1398 (2010).